On the Achievable Rate of OFDM with Index Modulation

Miaowen Wen, *Member, IEEE,* Xiang Cheng, *Senior Member, IEEE,* Meng Ma, Bingli Jiao, *Member, IEEE,* and H. Vincent Poor, *Fellow, IEEE*

***Abstract*—Orthogonal frequency division multiplexing with index modulation (OFDM-IM) is a recently developed transmission technique that extends the principle of spatial modulation to OFDM subcarriers. In this paper, the performance of OFDM-IM is studied in terms of the achievable rate assuming an M-ary constellation and that channel state information is available at the receiver. A closed-form lower bound is derived, based on which an interleaved grouping method is proposed for the use of subcarriers. In comparison with the existing grouping method, the proposed one can better benefit from the diversity effects over frequency-selective fading channels, especially when the spacing of any two subcarriers within a subcarrier group is larger than the coherence bandwidth. Through numerical results, it is revealed that OFDM-IM with interleaved grouping outperforms classical OFDM for small M and certain ranges of signal-to-noise ratio. Finally, the effects of modulation types on the performance of OFDM-IM are studied. It is found that the superiority of OFDM-IM over classical OFDM is greater for phase-shift keying than for quadrature amplitude modulation.**

***Index Terms*—Spatial modulation, OFDM, index modulation, achievable rate, capacity.**

I. Introduction

As a member of the single-radio-frequency (RF) large-scale multiple-input multiple-output (MIMO) family, spatial modulation (SM) has been receiving significant attention recently due to its potential to strike an attractive tradeoff between the spectral efficiency and the energy efficiency of a wireless network [1]–[6]. The basic idea of SM is to activate a subset of antennas to transmit information symbols and meanwhile use indices of the active antennas to implicitly convey information. SM is also well known for its special case, space shift keying (SSK), which transmits information by antenna activation only [7]–[9]. Several experimental studies have substantiated the potential benefits of SM [10]–[12], and it has been widely acknowledged that SM is an alternative to the well-known MIMO solutions, such as Vertical Bell Laboratories Layered Space-Time (V-BLAST) and space-time coding [3]. Orthogonal frequency division multiplexing (OFDM) is another promising technique, which has been already integrated into modern wireless communication standards, such as 3GPP Long Term Evolution (LTE) [13]. OFDM is favorable for broadband wireless communications since it has high spectral efficiency and can effectively combat the intersymbol interference caused by the frequency-selective fading channel.

Attentive to the potential of SM and OFDM, researchers have devoted significant recent effort to their combination. Generally, these existing work can be classified into two categories. In the first category, SM is simply applied to OFDM transmission (SM-OFDM) [14]–[16]. In particular, SM-OFDM groups the OFDM subcarriers occupying the same frequency band at all transmit antennas so that SM can operate on those subcarriers subject to independent fading due to sufficient spacing between antennas. Thereafter, all transmit antennas are activated to transmit the generated OFDM signals following the conventional MIMO-OFDM process. The performance of SM-OFDM has been theoretically studied and some positive results have been found [14]–[16]. In the second category, the principle of SM is extended to subcarrier activation in OFDM. The first scheme that exploited this idea was called subcarrier index modulation OFDM (SIM-OFDM) [17]. In SIM-OFDM, half of the subcarriers are activated according to the incoming information bits and some other subcarriers are dedicated to signaling. However, SIM-OFDM assumes perfect detection of the signaling at the receivers and suffers from bit error propagation. To solve this problem, an enhanced SIM-OFDM (ESIM-OFDM) scheme was later proposed in [18]. Unlike SIM-OFDM, ESIM-OFDM uses one bit to control two adjacent subcarriers such that only one subcarrier is activated at a time. At the receiver, the detection of the state of any subcarrier can be easily accomplished by comparing the power with that of its adjacent subcarrier. However, the spectral efficiency of ESIM-OFDM tends to be much smaller than that of classical OFDM when a high-order modulation is assumed for the symbols carried on the active subcarriers since the number of active subcarriers is fixed. The authors in [18] raised the idea of relaxing this limitation by allowing more subcarriers to be active. Unfortunately, no further attempt at practical implementation has been found.

The aforementioned incomplete work in [18] was carried out independently in [19], where the new scheme is named

This work was supported in part by the National Natural Science Foundation of China under Grants 61501190 and 61571020, the National 973 Project under Grant 2013CB336700, and the Natural Science Foundation of Guangdong Province under Grant 2014A030310389. This paper was presented in part at the IEEE International Conference on Intelligent Transportation Systems 2014, Qingdao, China, October 2014, and in part at the IEEE International Conference on Communication Systems, Macau, China, November 2014.

M. Wen is with School of Electronic and Information Engineering, South China University of Technology, Guangzhou 510641, China (e-mail: eemwwen@scut.edu.cn).

X. Cheng, M. Ma, and B. Jiao are with School of Electronics and Computer Science, Peking University, Beijing 100871, China (e-mail: {xiangcheng, mam, jiaobl}@pku.edu.cn).

H. V. Poor is with Department of Electrical Engineering, Princeton University, Princeton, NJ 08540, USA (email: poor@princeton.edu).

OFDM with index modulation (OFDM-IM). Specifically, to reduce the complexity lying in the selection of active subcarriers, the authors proposed an efficient one-to-one mapping that relates the incoming information bits with the active subcarrier indices based on combinatorial number theory. Moreover, a log-likelihood ratio (LLR) detector was also proposed to determine the active subcarriers and the modulated symbols, achieving not only near maximum likelihood (ML) performance but also identical computational complexity to that of the classical OFDM detector. More recently, further efforts on the theoretical analysis of the uncoded bit error rates (BERs) under perfect and imperfect channel estimation as well as the implementation of OFDM-IM with terminal mobility were made by the same authors in [20]. It is shown in [19] and [20] that since the transmit power of each active subcarrier is enhanced and the information bits conveyed by subcarrier activation can be used to compensate for the size of the signal constellation, OFDM-IM can achieve significantly better uncoded BER performance than classical OFDM.

The superior performance of OFDM-IM in terms of BER motivated our work. In this paper, we investigate the (ergodic) achievable rate of OFDM-IM assuming slowly varying Rayleigh fading channels and channel state information at the receiver (CSIR). We mainly focus on the analysis under an M-ary constellation constraint considering that a finite-alphabet input makes more practical sense [21]–[25], and briefly study the asymptotic case in which the constellation size tends to infinity. A closed-form lower bound on the constellation-constrained achievable rate is derived, which tracks very well the trend of the exact values as signal-to-noise ratio (SNR) increases and can be used to estimate many important parameters, such as the optimal number of (in)active subcarriers in maximizing the achievable rate. The contributions of this paper are summarized as follows.

- We propose a new subcarrier grouping method for OFDM-IM, which applies interleaved mapping [26]. The idea is motivated by the fact that interleaved grouping can better benefit from frequency-selective fading, which brings frequency diversity gain to OFDM-IM. An analytical proof and numerical results are presented to validate the superiority of the interleaved grouping over the existing localized grouping. We find that OFDM-IM with interleaved grouping can achieve SNR gain over classical OFDM under a low-order alphabet input. This improvement, however, becomes smaller as the alphabet size gets larger and is even lost when it increases further.
- We investigate the achievable rate of OFDM-IM with subcarrier activation only, which is a special case of OFDM-IM. We show that since the coding gain from subcarrier activation cannot compensate for the loss of spectral efficiency, OFDM-IM with subcarrier activation only exhibits poor performance. We also discuss the effects of modulation types on the achievable rate of OFDM-IM. It is found that the superiority of OFDM-IM over classical OFDM is greater for phase-shift keying (PSK) than for quadrature amplitude modulation (QAM).

The rest of this paper is outlined as follows. Section II describes the system model for OFDM-IM. In Section III, the achievable rates of OFDM-IM under constellation constraint and Gaussian inputs are derived, followed by the discussion of OFDM-IM with subcarrier activation only. Section IV proposes the interleaved grouping approach for OFDM-IM. Numerical results are presented in Section V. Finally, Section VI concludes the paper.

Notation: Upper and lower case boldface letters denote matrices and column vectors, respectively. Superscripts ^{T}, ^{H}, and $^{-1}$ stand for transpose, Hermitian transpose, and inversion operations, respectively. The (a,b)-th entry of matrix $\mathbf{X}$ is denoted by $[\mathbf{X}]_{a,b}$. $\mathrm{Tr}\{\mathbf{X}\}$ stands for the trace of matrix $\mathbf{X}$. $\mathrm{diag}\{\mathbf{x}\}$ creates a diagonal matrix whose diagonal elements are $\mathbf{x}$. $\mathrm{Re}\,(\cdot)$ and $\mathrm{Im}\,(\cdot)$ denote the real and the imaginary parts of a complex number, respectively. $|\cdot|$ denotes the absolute value if applied to a complex number or the cardinality if applied to a set. $\det(\cdot)$ denotes the determinant of a matrix. $E_x[\cdot]$ and $E_{\mathbf{x}}[\cdot]$ represent the expectations over a random variable (RV) x and a random vector $\mathbf{x}$, respectively. $\mathrm{C}(n,k)$ denotes the binomial coefficient. The probability density function (PDF) and the probability of an event are denoted by $f(\cdot)$ and $\Pr(\cdot)$, respectively. $\mathbf{I}_L$ and $\mathbf{0}_L$ represent the $L \times L$ identity and zero matrices, respectively. $\mathrm{H}(\cdot)$, $\mathrm{h}(\cdot)$, and $\mathrm{I}(\cdot,\cdot)$ denote the entropy, the differential entropy, and the mutual information, respectively. $\mathcal{S} = \{s_1, \ldots, s_M\}$ denotes a complex signal set of cardinality M and unit power. $\emptyset$ denotes the empty set. If $\Omega_j(r) = i$, then $\Omega_j^{-1}(i) = r$. $\sum_{p^{(n)}} = \sum_{p_1=1}^{M} \cdots \sum_{p_n=1}^{M}$.

II. System model

Suppose that the system bandwidth is B_T, which is occupied by a total of N OFDM subcarriers, i.e., the subcarrier spacing is $B_S = B_T/N$. In OFDM-IM, the N subcarriers are split into $G = N/L$ groups, each of which consists of L subcarriers. For group g, the subcarrier indices are given by

$$\Psi^g = \{\beta_1^g, \ldots, \beta_L^g\} \tag{1}$$

where $\beta_l^g \in \{1, \ldots, N\}$ with $g = 1, \ldots, G$ and $l = 1, \ldots, L$. Note that $\Psi^{g_1} \cap \Psi^{g_2} = \emptyset$ and $\Psi^1 \cup \cdots \cup \Psi^G = \{1, \ldots, N\}$, where $g_1, g_2 \in \{1, \ldots, G\}$ and $g_1 \neq g_2$. It is assumed that both the transmitter and the receiver have agreed on the subcarrier grouping in (1). The reason why subcarrier grouping is employed in OFDM-IM will be clarified in the sequel.

Fig. 1 depicts the OFDM-IM baseband transmitter structure. The source bits are equally split into G blocks, each of which consists of two parts. The bits associated with bit block g determine the states of all subcarriers and modulate the symbols carried on the active subcarriers within subcarrier group g. Specifically, m out of L subcarriers within the subcarrier group are set to be inactive according to the bits of the first part and the remaining $(L-m)$ subcarriers are activated to transmit $(L-m)$ M-ary PSK/QAM modulated symbols according to the bits of the second part. Note that given L and m, there are in total $\mathrm{C}(L,m)$ combinations of active/inactive subcarrier indices. Take $L = 4$ and $m = 2$ for example. All $\mathrm{C}(4,2) = 6$ combinations for subcarrier group

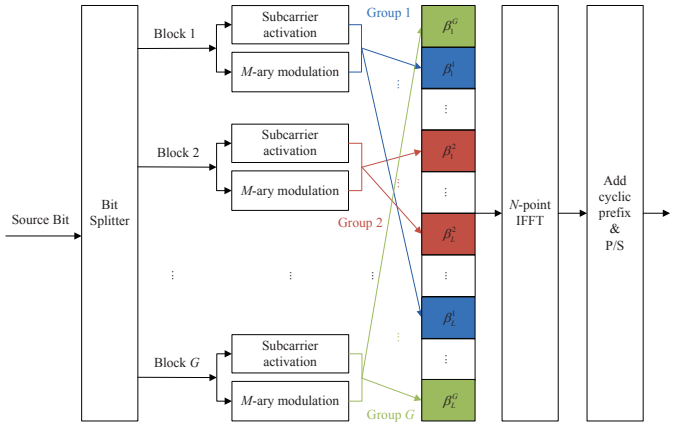

Fig. 1. Baseband transmitter structure of OFDM-IM with arbitrary grouping.

g are listed as follows:

$$\begin{aligned}
\Omega_1^g &= \{\beta_1^g, \beta_2^g\} \left(\overline{\Omega}_1^g = \{\beta_3^g, \beta_4^g\}\right), \\
\Omega_2^g &= \{\beta_1^g, \beta_3^g\} \left(\overline{\Omega}_2^g = \{\beta_2^g, \beta_4^g\}\right), \\
\Omega_3^g &= \{\beta_1^g, \beta_4^g\} \left(\overline{\Omega}_3^g = \{\beta_2^g, \beta_3^g\}\right), \\
\Omega_4^g &= \{\beta_2^g, \beta_3^g\} \left(\overline{\Omega}_4^g = \{\beta_1^g, \beta_4^g\}\right), \\
\Omega_5^g &= \{\beta_2^g, \beta_4^g\} \left(\overline{\Omega}_5^g = \{\beta_1^g, \beta_3^g\}\right), \\
\Omega_6^g &= \{\beta_3^g, \beta_4^g\} \left(\overline{\Omega}_6^g = \{\beta_1^g, \beta_2^g\}\right)
\end{aligned}$$

where Ω_j^g represents the j-th combination of the active subcarrier indices for subcarrier group g and $\overline{\Omega}_j^g$ is the complement of Ω_j^g with respect to the set Ψ^g, which therefore denotes the j-th combination of the inactive subcarrier indices for subcarrier group g. The way to select one out of $\mathrm{C}(L,m)$ combinations of active/insubcarrier indices according to random bits has been provided in [20], which is omitted here for brevity. Assume that the output of the index selector for active subcarriers is

$$\mathbf{x}_c^g \in \left\{\Omega_1^g, \ldots, \Omega_{\mathrm{C}(L,m)}^g\right\}. \tag{2}$$

Now, it is clear that subcarrier grouping is necessary for OFDM-IM since without it we have $L = N$ and $\mathrm{C}(N,m)$ can take very large values, which makes the implementation complexity of OFDM-IM high. On the other hand, assume that the vector of the modulated symbols at the output of the M-ary modulator is given by

$$\mathbf{x}_s^g \in \mathcal{S}^{L-m}. \tag{3}$$

Denote the total transmit power of the system as P_T. By taking into account $\mathbf{x}_c^g$ and $\mathbf{x}_s^g$ for all g and concatenating G subcarrier groups, the frequency-domain OFDM symbol is created as

$$\mathbf{x} = [x_1, \ldots, x_N]^T \tag{4}$$

where $x_i \in \{0, \sqrt{P_G/(L-m)}\mathbf{x}_s^1, \ldots, \sqrt{P_G/(L-m)}\mathbf{x}_s^G\}$ with $P_G = P_T/G$ representing the total transmit power within each subcarrier group and $i = 1, \ldots, N$. Note that as the transmitter has no knowledge of the channel state information (CSI), it is wise to allocate active subcarriers with equal power. Also note that the power allocated to each active subcarrier is $P_G/(L-m)$ for OFDM-IM rather than P_G/L for classical OFDM in order to balance the total transmit power. This policy is the so-called power reallocation in [17]. Before transmission, the inverse fast Fourier transform (IFFT) is applied to (4), yielding

$$\breve{x}_k = \frac{1}{\sqrt{N}} \sum_{i=1}^{N} x_i e^{\frac{2\sqrt{-1}\pi(i-1)(k-1)}{N}}, \quad k = 1, \ldots, N \tag{5}$$

and a length-Q cyclic prefix (CP) of samples $[\breve{x}_{N-Q+1}, \ldots, \breve{x}_N]^T$ is appended to the beginning of the time-domain main OFDM symbol $\breve{\mathbf{x}} = [\breve{x}_1, \ldots, \breve{x}_N]^T$.

Consider a slowly time-varying multipath Rayleigh fading channel with channel impulse response

$$\breve{\mathbf{h}} = \left[\breve{h}_1, \ldots, \breve{h}_D\right]^T \tag{6}$$

where D is the number of channel taps, and $\breve{h}_d$ $(d = 1, \ldots, D)$ is circularly symmetric complex Gaussian distributed with $E_{\breve{h}_d}[|\breve{h}_d|^2] = \delta_d^2$ and $E_{\breve{\mathbf{h}}}[\breve{\mathbf{h}}^H\breve{\mathbf{h}}] = \sum_{d=1}^{D}\delta_d^2 = 1$. Suppose that the CP length Q is no smaller than $D-1$. After the removal of the CP and the application of the FFT, the frequency-domain received signal on the i-th subcarrier is given by

$$y_i = x_i h_i + w_i, \quad i = 1, \ldots, N \tag{7}$$

where $h_i = \sum_{d=1}^{D} \breve{h}_d e^{-2\sqrt{-1}\pi(i-1)(d-1)/N}$ is the channel coefficient and w_i is additive white Gaussian noise (AWGN) of power σ^2 at the i-th subcarrier, whose vector representations are given by $\mathbf{h}$ and $\mathbf{w}$, respectively. Note that as the power delay profile is normalized, it follows that $E_{\mathbf{h}}\left[\mathbf{h}^H\mathbf{h}\right] = N$. Also note that $\sigma^2 = N_0 B_S$, where N_0 is the power spectral density of the AWGN. Finally, from (7), the active/inactive subcarrier indices and the modulated symbols for each subcarrier group can be jointly detected [20].

From the principle of OFDM-IM described above, one can discover that the index modulation always works efficiently even if all subcarriers are faded completely correlatively, i.e., $h_1 = \cdots = h_N$, thanks to the IFFT at the transmitter and the FFT at the receiver. This is quite different from the SM technique, which fails when the channels between different transmit antennas are highly correlated. Note that though we did not specify in (1) how to choose the subcarrier indices, a manner has been suggested in [20], which is

$$\Psi^g = \{\beta_1^g, \ldots, \beta_L^g\} = \{L(g-1)+1, \ldots, Lg\} \tag{8}$$

with $\beta_l^g = L(g-1)+l$, where $g = 1, \ldots, G$ and $l = 1, \ldots, L$. This means each set of L adjacent subcarriers forms a subcarrier group, as shown in Fig. 2. As this manner is similar to the localized mapping in LTE systems [26], it is termed localized grouping in this paper.

Since OFDM-IM is in essence a kind of OFDM transmission technique, we are interested in its performance behavior and the comparison with classical OFDM. Specifically, we aim at answering the following questions from an information-theoretic perspective in this paper:

- *Q1*: Is there a better subcarrier grouping method than localized grouping for OFDM-IM?
- *Q2*: Can OFDM-IM outperform classical OFDM in the case of $L = M$?
- *Q3*: How does the special case of OFDM-IM, i.e., OFDM-IM with subcarrier activation only, perform?
- *Q4*: What is the optimal subcarrier activation strategy for OFDM-IM in the case of $L = M$?
- *Q5*: How does the performance superiority of OFDM-IM over classical OFDM behave for different modulation types?

Note that the condition in *Q2* and *Q4* is of particular interest since given M-ary constellation input OFDM-IM shares the same entropy at the channel input with classical OFDM by inactivating one out of L subcarriers [28].

III. Analysis of Achievable Rate

In this section, we investigate the (ergodic) achievable rate of OFDM-IM assuming CSIR. For fair comparison between OFDM-IM and classical OFDM, we resort to a unified definition of SNR as $\gamma = P_T/N_0B_T = P_G/L\sigma^2$. The achievable rate of OFDM-IM is defined as [29]

$$\begin{aligned} R_{\mathrm{OFDM-IM}}(\gamma) &= \frac{1}{B_T}\left(B_S E_{\mathbf{h}}\left[\mathrm{I}(\mathbf{x};\mathbf{y}|\mathbf{h})\right]\right) \\ &= \frac{1}{N} E_{\mathbf{h}}\left[\mathrm{I}(\mathbf{x};\mathbf{y}|\mathbf{h})\right]. \end{aligned} \tag{9}$$

Note that (9) is exactly the spectral efficiency of OFDM-IM, measured in bits per second per Hertz (bps/Hz) [30]. For simplicity, we restrict our analysis to the OFDM-IM system with regular subcarrier grouping, which implies that the frequency correlation is the same for all subcarrier groups, though it can be easily extended to arbitrary subcarrier grouping. An example for regular subcarrier grouping is the existing localized grouping, since under this method the (a,b)-th entry of the covariance matrix of $\mathbf{h}^g$, defined as $\mathbf{\Sigma} = E_{\mathbf{h}^g}[\mathbf{h}^g(\mathbf{h}^g)^H]$, equals $[\mathbf{\Sigma}_{\mathrm{LG}}]_{a,b} = \sum_{d=1}^{D}\delta_d^2 e^{-2\sqrt{-1}\pi(a-b)(d-1)/N}$ with $a, b = 1,\ldots,L$, which does not depend on g. Now, under the assumption of regular subcarrier grouping and based on the fact that the encoding and decoding processes associated with each subcarrier group are identical and statistically independent, (9) can be simplified as

$$\begin{aligned} R_{\mathrm{OFDM-IM}}(\gamma) &= \frac{1}{N}\sum_{g'=1}^{G} E_{\mathbf{h}^{g'}}\left[\mathrm{I}\left(\mathbf{x}^{g'};\mathbf{y}^{g'}|\mathbf{h}^{g'}\right)\right] \\ &= \frac{1}{L} E_{\mathbf{h}^g}\left[\mathrm{I}\left(\mathbf{x}_s^g,\mathbf{x}_c^g;\mathbf{y}^g|\mathbf{h}^g\right)\right],\ \forall g \in \{1,\ldots,G\}. \end{aligned} \tag{10}$$

According to (10), in the sequel we will only focus on one subcarrier group for achievable rate analysis. For brevity, we omit the superscript g for all variables defined above. In addition, we let $\beta_l = l$ for notational simplicity such that all subcarriers within the subcarrier group will be indexed from $\{1,\ldots,L\}$. Note that with the above notation, we will refer to the i-th subcarrier simply as the β_i-th subcarrier of OFDM signals unless otherwise specified.

A. Finite constellation input

In this subsection, $\mathbf{x}_s$ is considered to be a finite signal set, i.e., M is finite. However, for practical interests, we restrict the signal set to be a discrete constellation, such as M-ary PSK or QAM, where the constellation points are equiprobable.

Proposition 1: The achievable rate of OFDM-IM is given by

$$\begin{aligned} R_{\mathrm{OFDM-IM}}(\gamma) =& \frac{L-m}{L}\log_2(M) + \frac{\log_2\left(\mathrm{C}(L,m)\right)}{L} \\ &- \left(\log_2(e) - 1\right) - \lambda(\gamma) \end{aligned} \tag{11}$$

with

$$\begin{aligned} \lambda(\gamma) =& \frac{1}{LM^{L-m}\mathrm{C}(L,m)} \sum_{j=1}^{\mathrm{C}(L,m)} \sum_{p^{(L-m)}} \\ &\times E_{\mathbf{v},\mathbf{h}}\left[\log_2\left(\sum_{j'=1}^{\mathrm{C}(L,m)} \sum_{p'^{(L-m)}} \prod_{i=1}^{L} \xi(v_i,h_i,\gamma)\right)\right] \end{aligned} \tag{12}$$

where $\xi(v_i,h_i,\gamma)$ is given in (13), shown at the top of the next page, and $\mathbf{v} = [v_1,\ldots,v_L]^T$ is a complex Gaussian random vector with covariance $\mathbf{I}_L$.

Proof: From (10), the achievable rate of OFDM-IM is given by

$$R_{\mathrm{OFDM-IM}}(\gamma) = \tfrac{1}{L}\left[\mathrm{H}(\mathbf{x}_s,\mathbf{x}_c) - E_{\mathbf{h}}\left[\mathrm{H}(\mathbf{x}_s,\mathbf{x}_c|\mathbf{y},\mathbf{h})\right]\right] \tag{14a}$$

$$= \tfrac{L-m}{L}\log_2(M) + \tfrac{\log_2(\mathrm{C}(L,m))}{L} - \tfrac{1}{L}E_{\mathbf{h}}\left[\mathrm{H}(\mathbf{x}_s,\mathbf{x}_c|\mathbf{y},\mathbf{h})\right] \tag{14b}$$

where (14a) is derived according to the definition of mutual information [31] and (14b) holds due to the independence between symbol modulation and subcarrier activation. Towards computing (10), we turn to calculate $E_{\mathbf{h}}[\mathrm{H}(\mathbf{x}_s,\mathbf{x}_c|\mathbf{y},\mathbf{h})]$ in favor of (14b). First, let us express $\mathrm{H}(\mathbf{x}_s,\mathbf{x}_c|\mathbf{y},\mathbf{h})$ according to its definition [31] as (15), shown at the top of the next page, where $\mathbf{s} = [s_{p_1},\ldots,s_{p_{L-m}}]^T \in \mathcal{S}^{L-m}$, $\Pr(\mathbf{x}_c = \Omega_j, \mathbf{x}_s = \mathbf{s}) = 1/\mathrm{C}(L,m)M^{L-m}$,

$$\begin{aligned} f(\mathbf{y}|\mathbf{x}_c = \Omega_j, \mathbf{x}_s = \mathbf{s}, \mathbf{h}) =& \frac{1}{\left(\pi\sigma^2\right)^L} \prod_{i=1}^{m} e^{-\frac{\left|y_{\bar{\Omega}_j(i)}\right|^2}{\sigma^2}} \\ &\times \prod_{i=1}^{L-m} e^{-\frac{\left|y_{\Omega_j(i)} - h_{\Omega_j(i)}\sqrt{\frac{P_G}{L-m}}s_{p_i}\right|^2}{\sigma^2}} \end{aligned} \tag{16}$$

and

$$\begin{aligned} f(\mathbf{y}|\mathbf{h}) =& \frac{\left(\pi\sigma^2\right)^{-L}}{\mathrm{C}(L,m)M^{L-m}} \sum_{j'=1}^{\mathrm{C}(L,m)} \sum_{p'^{(L-m)}} \prod_{i'=1}^{m} e^{-\frac{\left|y_{\bar{\Omega}_{j'}(i')}\right|^2}{\sigma^2}} \\ &\times \prod_{i'=1}^{L-m} e^{-\frac{\left|y_{\Omega_{j'}(i')} - h_{\Omega_{j'}(i')}\sqrt{\frac{P_G}{L-m}}s_{p'_{i'}}\right|^2}{\sigma^2}}. \end{aligned} \tag{17}$$

Then, changing the integral variables in (15) by

$$v_i = \begin{cases} (y_i - h_i x_i)/\sigma, & i \in \Omega_j \\ y_i/\sigma, & i \in \bar{\Omega}_j \end{cases} \tag{18}$$

(15) can be reformulated as (19), shown at the top of the next page, where $\mathbf{v} = [v_1,\ldots,v_L]^T$ and $f(\mathbf{v}) = \pi^{-L}e^{-\|\mathbf{v}\|^2}$ from (18). Since extracting the coefficient $1/2$ from the first term at the right hand side of (19) yields $-L$ and the integral in

$$\xi\left(v_i,h_i,\gamma\right)=\begin{cases}2e^{-\left|v_i+h_i\sqrt{\frac{\gamma L}{L-m}}\left(s_{p_{\Omega_j^{-1}(i)}}-s_{p'_{\Omega_{j'}^{-1}(i)}}\right)\right|^2}, & i\in\Omega_j\cap\Omega_{j'}\\ 2e^{-\left|v_i+h_i\sqrt{\frac{\gamma L}{L-m}}s_{p_{\Omega_j^{-1}(i)}}\right|^2}, & i\in\Omega_j\cap\overline{\Omega}_{j'}\\ 2e^{-\left|v_i-h_i\sqrt{\frac{\gamma L}{L-m}}s_{p'_{\Omega_{j'}^{-1}(i)}}\right|^2}, & i\in\overline{\Omega}_j\cap\Omega_{j'}\\ 2e^{-|v_i|^2}, & i\in\overline{\Omega}_j\cap\overline{\Omega}_{j'}\end{cases} \tag{13}$$

$$\begin{aligned}\mathrm{H}\left(\mathbf{x}_s,\mathbf{x}_c|\mathbf{y},\mathbf{h}\right)=-\sum_{j=1}^{\mathrm{C}(L,m)}\sum_{p^{(L-m)}}\int_{\mathbf{y}}\Pr\left(\mathbf{x}_c=\Omega_j,\mathbf{x}_s=\mathbf{s}\right)f\left(\mathbf{y}|\mathbf{x}_c=\Omega_j,\mathbf{x}_s=\mathbf{s},\mathbf{h}\right)\\ \times\log_2\left(\frac{\Pr\left(\mathbf{x}_c=\Omega_j,\mathbf{x}_s=\mathbf{s}\right)f\left(\mathbf{y}|\mathbf{x}_c=\Omega_j,\mathbf{x}_s=\mathbf{s},\mathbf{h}\right)}{f\left(\mathbf{y}|\mathbf{h}\right)}\right)d\mathbf{y}\end{aligned} \tag{15}$$

$$\begin{aligned}\mathrm{H}\left(\mathbf{x}_s,\mathbf{x}_c|\mathbf{y},\mathbf{h}\right)=&\frac{1}{M^{L-m}\mathrm{C}\left(L,m\right)}\sum_{j=1}^{\mathrm{C}(L,m)}\sum_{p^{(L-m)}}\int_{\mathbf{v}}f\left(\mathbf{v}\right)\log_2\left(\sum_{j'=1}^{\mathrm{C}(L,m)}\sum_{p'^{(L-m)}}\prod_{i=1}^{L}\frac{\xi\left(v_i,h_i,\gamma\right)}{2}\right)d\mathbf{v}\\ &+\frac{1}{M^{L-m}\mathrm{C}\left(L,m\right)}\sum_{j=1}^{\mathrm{C}(L,m)}\sum_{p^{(L-m)}}\int_{\mathbf{v}}f\left(\mathbf{v}\right)\log_2\left(\frac{1}{f\left(\mathbf{v}\right)}\right)d\mathbf{v}-L\log_2\left(\pi\right)\end{aligned} \tag{19}$$

the second term gives the differential entropy of $\mathbf{v}$, $\mathrm{h}\left(\mathbf{v}\right)=L\log_2\left(\pi e\right)$, we have

$$\frac{1}{L}E_{\mathbf{h}}\left[\mathrm{H}\left(\mathbf{x}_s,\mathbf{x}_c|\mathbf{y},\mathbf{h}\right)\right]=\log_2\left(e\right)-1+\lambda\left(\gamma\right). \tag{20}$$

Finally, substituting (20) into (14b) completes the proof. ■

Remark 1: For the case that OFDM-IM has full subcarrier-correlations, i.e., $h_1=\cdots=h_L$, the expectation over $\mathbf{h}$ in (11) is simplified to an expectation over a single random variable. However, it should be noted that the resulting achievable rate is larger than $\log_2(M)(L-m)/L$ at high SNR, which will be validated in the following Corollary 1. Also note that unlike classical OFDM, for a given channel realization the received signals on different subcarriers become dependent in OFDM-IM. This is true as $f\left(\mathbf{y}|\mathbf{h}\right)\neq\prod_{i=1}^{L}f\left(y_i|h_i\right)$, where

$$f\left(y_i|h_i\right)=\frac{1}{\pi\sigma^2}\left(\frac{L-m}{LM}\sum_{\forall s\in\mathcal{S}}e^{-\frac{\left|y_i-h_i\sqrt{\frac{P_G}{L-m}}s\right|^2}{\sigma^2}}+\frac{m}{L}e^{-\frac{|y_i|^2}{\sigma^2}}\right) \tag{21}$$

with $i=1,\ldots,L$.

Corollary 1: When SNR approaches 0 and $+\infty$, the achievable rates of OFDM-IM tend to

$$\lim_{\gamma\to0}R_{\mathrm{OFDM-IM}}\left(\gamma\right)=0 \tag{22}$$

and

$$\begin{aligned}&\lim_{\gamma\to+\infty}R_{\mathrm{OFDM-IM}}\left(\gamma\right)\\ &=\frac{L-m}{L}\log_2\left(M\right)+\frac{\log_2\left(\mathrm{C}\left(L,m\right)\right)}{L}\end{aligned} \tag{23}$$

respectively.

Proof: First, consider $\gamma\to0$. In this case, we have $\lim_{\gamma\to0}\xi\left(v_i,h_i,\gamma\right)=2e^{-|v_i|^2}$ from (13) and

$$\begin{aligned}\lim_{\gamma\to0}\lambda\left(\gamma\right)=&\frac{1}{LM^{L-m}\mathrm{C}\left(L,m\right)}\sum_{j=1}^{\mathrm{C}(L,m)}\sum_{p^{(L-m)}}\\ &\times E_{\mathbf{v}}\left[\log_2\left(2^Le^{-\|\mathbf{v}\|^2}\mathrm{C}\left(L,m\right)M^{L-m}\right)\right]\\ =&\frac{L-m}{L}\log_2\left(M\right)+\frac{\log_2\left(\mathrm{C}\left(L,m\right)\right)}{L}-\left(\log_2\left(e\right)-1\right)\end{aligned} \tag{24}$$

from (12). Then, substituting (24) into (11) yields (22). Second, consider $\gamma\to+\infty$. Let $\mu\left(j,j',\mathbf{p},\mathbf{p}'\right)=|j-j'|+\|\mathbf{p}-\mathbf{p}'\|$, where $\mathbf{p}=[p_1,\ldots,p_{L-m}]^T$ and $\mathbf{p}'=[p'_1,\ldots,p'_{L-m}]^T$. Then, (12) can be rewritten as (25), shown at the top of the next page. Since for $\mu\left(j,j',\mathbf{p},\mathbf{p}'\right)\neq0$ we always have at least an element, i, which belongs to $\left(\Omega_j\cap\Omega_{j'}\right)\cup\left(\Omega_j\cap\bar{\Omega}_{j'}\right)\cup\left(\bar{\Omega}_j\cap\Omega_{j'}\right)$, satisfying $\lim_{\gamma\to+\infty}\xi\left(v_i,h_i,\gamma\right)=0$ from (13), the second term inside the logarithmic function in (25) approaches zero for $\gamma\to+\infty$. Therefore, it follows that $\lim_{\gamma\to+\infty}\lambda\left(\gamma\right)=1-\log_2\left(e\right)$, which, when substituted into (11), makes (23) valid. ■

Remark 2: Corollary 1 is intuitive. When SNR is very small, the transmitted information is seriously contaminated by noise and thus no rate can be guaranteed by the channel. On the contrary, when SNR is very large, all transmitted information can be transferred through the channel with an arbitrarily low probability of error and thus the achievable rate is limited to the entropy at the channel input.

$$\lambda\left(\gamma\right)=\frac{M^{m-L}}{L\mathrm{C}\left(L,m\right)}\sum_{j=1}^{\mathrm{C}(L,m)}\sum_{p^{(L-m)}}E_{\mathbf{v},\mathbf{h}}\left[\log_2\left(2^Le^{-\|\mathbf{v}\|^2}+\underbrace{\sum_{j'=1}^{\mathrm{C}(L,m)}\sum_{p'^{(L-m)}}}_{\mu(j,j',\mathbf{p},\mathbf{p}')\neq0}\prod_{i=1}^{L}\xi\left(v_i,h_i,\gamma\right)\right)\right]. \tag{25}$$

To the best of our knowledge, no closed-form result exists for (11). Consequently, we have to calculate it based on the Monte-Carlo method, which, however, need not guarantee accuracy [27]. Note that besides Monte-Carlo simulations, one can also obtain an approximation of (11) by following the method proposed in [25]. However, extensive computations are needed to estimate the gradient of (11).

1) Lower bound: To circumvent the above problems, we derive a closed-form lower bound in the sequel.

Proposition 2: The achievable rate of OFDM-IM is lower bounded by

$$\begin{aligned}R^{\mathrm{L}}_{\mathrm{OFDM-IM}}\left(\gamma\right)\triangleq&\frac{L-m}{L}\log_2\left(M\right)+\frac{\log_2\left(\mathrm{C}\left(L,m\right)\right)}{L}\\&-\left(\log_2\left(e\right)-1\right)-\frac{1}{L\mathrm{C}\left(L,m\right)}\\&\times\frac{1}{M^{L-m}}\sum_{j=1}^{\mathrm{C}(L,m)}\sum_{p^{(L-m)}}\log_2\left(\sum_{j'=1}^{\mathrm{C}(L,m)}\right.\\&\left.\times\sum_{p'^{(L-m)}}\frac{1}{\det\left(\mathbf{I}_L+\mathbf{\Sigma}\mathbf{\Lambda}_{j,j'}\right)}\right)\end{aligned} \tag{26}$$

where $\mathbf{\Lambda}_{j,j'}$ is an $L\times L$ diagonal matrix whose i-th diagonal element is given by

$$\left[\mathbf{\Lambda}_{j,j'}\right]_{i,i}=\begin{cases}\frac{\gamma L}{L-m}\frac{\left|s_{p_{\Omega_j^{-1}(i)}}-s_{p'_{\Omega_{j'}^{-1}(i)}}\right|^2}{2}, & i\in\Omega_j\cap\Omega_{j'}\\ \frac{\gamma L}{L-m}\frac{\left|s_{p_{\Omega_j^{-1}(i)}}\right|^2}{2}, & i\in\Omega_j\cap\overline{\Omega}_{j'}\\ \frac{\gamma L}{L-m}\frac{\left|s_{p'_{\Omega_{j'}^{-1}(i)}}\right|^2}{2}, & i\in\overline{\Omega}_j\cap\Omega_{j'}\\ 0, & i\in\overline{\Omega}_j\cap\overline{\Omega}_{j'}\end{cases} \tag{27}$$

with $i=1,\ldots,L$.

Proof: The proof is somewhat similar to that in [37, Appendix B]. Thus, we only provide some intermediate steps toward the result. Since $\log_2\left(\cdot\right)$ is a concave function, applying Jensen's inequality to (12) gives

$$\begin{aligned}\lambda\left(\gamma\right)\leq&\frac{1}{LM^{L-m}\mathrm{C}\left(L,m\right)}\sum_{j=1}^{\mathrm{C}(L,m)}\sum_{p^{(L-m)}}\log_2\left(\sum_{j'=1}^{\mathrm{C}(L,m)}\right.\\&\left.\times\sum_{p'^{(L-m)}}E_{\mathbf{h}}\left[\prod_{i=1}^{L}E_{v_i}\left[\xi\left(v_i,h_i,\gamma\right)\right]\right]\right)\end{aligned} \tag{28}$$

where we have resorted to the property that $\mathbf{v}$ is independent of $\mathbf{h}$. Thanks to the integral result in [32, Eq. (3.323.2)], the inner expectation in (28) can be solved as (29), shown at the top of this page. Then, introducing the matrix $\mathbf{\Lambda}_{j,j'}$, we can express $\prod_{i=1}^{L}E_{v_i}\left[\xi\left(v_i,h_i,\gamma\right)\right]$ according to (29) as $e^{-\mathbf{h}^H\mathbf{\Lambda}_{j,j'}\mathbf{h}}$. Finally, the expectation over $\mathbf{h}$ in (28) can be solved in closed form as

$$\begin{aligned}E_{\mathbf{h}}\left[\prod_{i=1}^{L}E_{v_i}\left[\xi\left(v_i,h_i,\gamma\right)\right]\right]&=\frac{\pi^{-L}}{\det\left(\mathbf{\Sigma}\right)}\int_{\mathbf{h}}e^{-\mathbf{h}^H\left(\mathbf{\Sigma}^{-1}+\mathbf{\Lambda}_{j,j'}\right)\mathbf{h}}d\mathbf{h}\\&=\frac{1}{\det\left(\mathbf{I}_L+\mathbf{\Sigma}\mathbf{\Lambda}_{j,j'}\right)}\end{aligned} \tag{30}$$

which, when substituted into (28) and then into (11), proves (26). ∎

Corollary 2: When all subcarriers within a subcarrier group are faded completely correlatively, the proposed lower bound becomes

$$\begin{aligned}R^{\mathrm{L}}_{\mathrm{OFDM-IM-FC}}\left(\gamma\right)\triangleq&\frac{L-m}{L}\log_2\left(M\right)+\frac{\log_2\left(\mathrm{C}\left(L,m\right)\right)}{L}\\&-\left(\log_2\left(e\right)-1\right)-\frac{1}{L\mathrm{C}\left(L,m\right)}\\&\times\frac{1}{M^{L-m}}\sum_{j=1}^{\mathrm{C}(L,m)}\sum_{p^{(L-m)}}\log_2\left(\sum_{j'=1}^{\mathrm{C}(L,m)}\right.\\&\left.\times\sum_{p'^{(L-m)}}\frac{1}{1+\mathrm{Tr}\left\{\mathbf{\Lambda}_{j,j'}\right\}}\right).\end{aligned} \tag{31}$$

Proof: In the case of $h_1=\cdots=h_L$, $\mathbf{\Sigma}$ becomes an all-ones matrix and $\det\left(\mathbf{I}_L+\mathbf{\Sigma}\mathbf{\Lambda}_{j,j'}\right)=1+\mathrm{Tr}\left\{\mathbf{\Lambda}_{j,j'}\right\}$, which, when substituted into (26), proves (31). ∎

Corollary 3: When SNR approaches 0 and $+\infty$, the proposed lower bounds tend to

$$\lim_{\gamma\to0}R^{\mathrm{L}}_{\mathrm{OFDM-IM}}\left(\gamma\right)=-\left(\log_2\left(e\right)-1\right) \tag{32}$$

and

$$\begin{aligned}&\lim_{\gamma\to+\infty}R^{\mathrm{L}}_{\mathrm{OFDM-IM}}\left(\gamma\right)\\&=\frac{L-m}{L}\log_2\left(M\right)+\frac{\log_2\left(\mathrm{C}\left(L,m\right)\right)}{L}-\left(\log_2\left(e\right)-1\right)\end{aligned} \tag{33}$$

respectively.

Proof: For $\gamma\to0$, we have $\mathbf{\Lambda}_{j,j'}\to\mathbf{0}_L$. Therefore, (32)

$$E_{v_i}\left[\xi\left(v_i,h_i,\gamma\right)\right]=\begin{cases} e^{-\frac{\gamma L}{L-m}\frac{|h_i|^2\left|s_{p_{\Omega_j^{-1}(i)}}-s_{p'_{\Omega_{j'}^{-1}(i)}}\right|^2}{2}}, & i\in\Omega_j\cap\Omega_{j'} \\ e^{-\frac{\gamma L}{L-m}\frac{|h_i|^2\left|s_{p_{\Omega_j^{-1}(i)}}\right|^2}{2}}, & i\in\Omega_j\cap\overline{\Omega}_{j'} \\ e^{-\frac{\gamma L}{L-m}\frac{|h_i|^2\left|s_{p'_{\Omega_{j'}^{-1}(i)}}\right|^2}{2}}, & i\in\overline{\Omega}_j\cap\Omega_{j'} \\ 1, & i\in\overline{\Omega}_j\cap\overline{\Omega}_{j'} \end{cases}. \tag{29}$$

holds from (26). On the other hand, for $\gamma\to+\infty$, we have

$$\begin{aligned}&\lim_{\gamma\to+\infty}\sum_{j'=1}^{\mathrm{C}(L,m)}\sum_{p'^{(L-m)}}\frac{1}{\det\left(\mathbf{I}_L+\mathbf{\Sigma}\mathbf{\Lambda}_{j,j'}\right)}\\&=1+\lim_{\gamma\to+\infty}\underbrace{\sum_{j'=1}^{\mathrm{C}(L,m)}\sum_{p'^{(L-m)}}}_{\mu(j,j',\mathbf{p},\mathbf{p}')\neq0}\frac{1}{\det\left(\mathbf{I}_L+\mathbf{\Sigma}\mathbf{\Lambda}_{j,j'}\right)}\\&=1.\end{aligned}\tag{34}$$

Therefore, (33) holds from (26). ∎

Remark 3: From Corollary 1 and Corollary 3, a constant gap, i.e., $-\left(\log_2\left(e\right)-1\right)$, between $R_{\mathrm{OFDM-IM}}\left(\gamma\right)$ and $R^{\mathrm{L}}_{\mathrm{OFDM-IM}}\left(\gamma\right)$ will be expected in both low and high SNR regions. However, as we will see in Section V, this does not apply to the remaining SNR region. In other words, approximating the exact value by shifting the lower bound by $\left(\log_2\left(e\right)-1\right)$ as [24] suggested does not work well to our case. Despite this, it will be shown in Section V that $R^{\mathrm{L}}_{\mathrm{OFDM-IM}}\left(\gamma\right)$ tracks very well the trend of $R_{\mathrm{OFDM-IM}}\left(\gamma\right)$ with the increase of SNR and can be used to estimate some parameters of practical interest with satisfactory accuracy.

From (26), it is clear that the achievable rate of OFDM-IM not only depends on the channel correlation, which is controlled by $\mathbf{\Sigma}$, but also on the modulation type, which determines $\mathbf{\Lambda}_{j,j'}$. An example for the former issue has been presented in Corollary 2. In the subsequent sections, both issues will be discussed in more detail.

2) Special case with $M=1$: When only subcarrier activation is applied in OFDM-IM [19], the resulting achievable rate can be expressed as (35), shown at the top of the next page, which follows from (11) by setting $M=1$. Also, a closed-form lower bound exists by letting $M=1$ in (26):

$$\begin{aligned}R^{\mathrm{L}}_{\mathrm{OFDM-IM-SC}}\left(\gamma\right)=&\frac{\log_2\left(\mathrm{C}\left(L,m\right)\right)}{L}-\left(\log_2\left(e\right)-1\right)\\&-\frac{1}{L\mathrm{C}\left(L,m\right)}\sum_{j=1}^{\mathrm{C}(L,m)}\log_2\left(\sum_{j'=1}^{\mathrm{C}(L,m)}\frac{1}{\left|\mathbf{I}_L+\mathbf{\Sigma}\mathbf{\Gamma}_{j,j'}\right|}\right)\end{aligned}\tag{36}$$

where $\mathbf{\Gamma}_{j,j'}$ is an $L\times L$ diagonal matrix whose i-th diagonal element is

$$\left[\mathbf{\Gamma}_{j,j'}\right]_{i,i}=\begin{cases}0, & i\in\left(\Omega_j\cap\Omega_{j'}\right)\cup\left(\bar{\Omega}_j\cap\bar{\Omega}_{j'}\right)\\ \frac{\gamma L}{2(L-m)}, & i\in\left(\bar{\Omega}_j\cap\Omega_{j'}\right)\cup\left(\Omega_j\cap\bar{\Omega}_{j'}\right)\end{cases}\tag{37}$$

with $i=1,\ldots,L$.

Recalling that on-off keying (OOK) transmits information by the intensity of the signal [33], we can readily determine that the OFDM-IM with subcarrier activation only is in fact an application of OOK modulation to OFDM subcarriers. Similarly, we can also apply OOK modulation to each subcarrier independently, thus generating a new scheme called OOK-OFDM. In Section V, we will compare the performance of the two aforementioned schemes.

B. Infinite constellation input

In this subsection, $\mathbf{x}_s$ is considered to be an infinite signal set, i.e., M is infinite. However, we restrict the signal set to be Gaussian, since it enables OFDM-IM to reach the supremum of all achievable rates [31], [34].

To begin with the derivation for the ergodic capacity of OFDM-IM, we first look into the conditional capacity of OFDM-IM on the channel, which can be expressed according to the chain rule for mutual information [31] as

$$\begin{aligned}C_{\mathrm{OFDM-IM}}\left(\gamma\right)&=\frac{1}{L}\mathrm{I}\left(\mathbf{x}_s,\mathbf{x}_c;\mathbf{y}|\mathbf{h}\right)\\&=\frac{1}{L}\left[\mathrm{I}\left(\mathbf{x}_s;\mathbf{y}|\mathbf{x}_c,\mathbf{h}\right)+\mathrm{I}\left(\mathbf{x}_c;\mathbf{y}|\mathbf{h}\right)\right].\end{aligned}\tag{38}$$

In (38), the first term at the right hand side is given by

$$\begin{aligned}\frac{\mathrm{I}\left(\mathbf{x}_s;\mathbf{y}|\mathbf{x}_c,\mathbf{h}\right)}{L}&=\frac{1}{L}\sum_{j=1}^{\mathrm{C}(L,m)}\Pr\left(\mathbf{x}_c=\Omega_j\right)\mathrm{I}\left(\mathbf{x}_s;\mathbf{y}|\mathbf{x}_c=\Omega_j,\mathbf{h}\right)\\&=\frac{1}{L\mathrm{C}\left(L,m\right)}\sum_{j=1}^{\mathrm{C}(L,m)}\sum_{i\in\Omega_j}\log_2\left(1+\frac{\gamma|h_i|^2L}{L-m}\right)\\&=\frac{L-m}{L^2}\sum_{i=1}^{L}\log_2\left(1+\frac{\gamma|h_i|^2L}{L-m}\right)\end{aligned}\tag{39}$$

where the last equality follows from the fact that each subcarrier is activated with probability $\left(L-m\right)/L$. It is clear from (39) that the degrees of freedom associated with OFDM-IM reduce to $\left(L-m\right)$ as opposed to L associated with classical OFDM, but OFDM-IM contributes a power gain of $L/(L-m)>1$. From (38), we see that in addition to this power gain, OFDM-IM also introduces a portion of information rate from subcarrier activation, i.e., the second

$$R_{\mathrm{OFDM-IM-SC}}(\gamma) = \frac{\log_2(\mathrm{C}(L,m))}{L} - (\log_2(e)-1) - \frac{1}{L\mathrm{C}(L,m)} \sum_{j=1}^{\mathrm{C}(L,m)} E_{\mathbf{v},\mathbf{h}} \left[\log_2 \left(\sum_{j'=1}^{\mathrm{C}(L,m)} \times \prod_{i \in (\Omega_j \cap \Omega_{j'}) \cup (\bar{\Omega}_j \cap \bar{\Omega}_{j'})} 2e^{-|v_i|^2} \prod_{i \in \Omega_j \cap \bar{\Omega}_{j'}} 2e^{-\left|v_i + h_i \sqrt{\frac{\gamma L}{L-m}}\right|^2} \prod_{i \in \bar{\Omega}_j \cap \Omega_{j'}} 2e^{-\left|v_i - h_i \sqrt{\frac{\gamma L}{L-m}}\right|^2} \right) \right] \quad (35)$$

term at the right hand side:

$$\frac{1}{L}\mathrm{I}(\mathbf{x}_c;\mathbf{y}|\mathbf{h}) = \frac{1}{L\mathrm{C}(L,m)} \sum_{j=1}^{\mathrm{C}(L,m)} \int_{\mathbf{y}} f(\mathbf{y}|\mathbf{x}_c = \Omega_j, \mathbf{h}) \times \log_2 \left(\frac{f(\mathbf{y}|\mathbf{x}_c = \Omega_j, \mathbf{h})}{f(\mathbf{y}|\mathbf{h})} \right) d\mathbf{y} \quad (40)$$

where

$$f(\mathbf{y}|\mathbf{x}_c = \Omega_j, \mathbf{h}) = \frac{1}{(\pi\sigma^2)^L} \prod_{i \in \Omega_j} \frac{1}{1+\gamma|h_i|^2 L/(L-m)} \times e^{-\frac{|y_i|^2}{\sigma^2\left[1+\gamma|h_i|^2 L/(L-m)\right]}} \prod_{i \in \bar{\Omega}_j} e^{-\frac{|y_i|^2}{\sigma^2}} \quad (41)$$

and

$$\begin{aligned} f(\mathbf{y}|\mathbf{h}) &= \sum_{j=1}^{\mathrm{C}(L,m)} \Pr(\mathbf{x}_c = \Omega_j) f(\mathbf{y}|\mathbf{x}_c = \Omega_j, \mathbf{h}) \\ &= \frac{1}{\mathrm{C}(L,m)(\pi\sigma^2)^L} \sum_{j=1}^{\mathrm{C}(L,m)} \prod_{i \in \Omega_j} \frac{1}{1+\gamma|h_i|^2 L/(L-m)} \\ &\quad \times e^{-\frac{|y_i|^2}{\sigma^2\left[1+\gamma|h_i|^2 L/(L-m)\right]}} \prod_{i \in \bar{\Omega}_j} e^{-\frac{|y_i|^2}{\sigma^2}}. \end{aligned} \quad (42)$$

According to the above analysis, one can expect that the instantaneous capacity of OFDM-IM will be smaller than that of the classical OFDM at high SNR due to the reduction in degrees of freedom. However, as OFDM-IM benefits from a power gain and additional information rate transferred via subcarrier activation, it is not clear whether OFDM-IM can outperform classical OFDM or not at low-to-medium SNR. The answer is given in the following proposition.

Proposition 3: The instantaneous capacity of OFDM-IM is smaller than that of classical OFDM over the entire SNR region:

$$C_{\mathrm{OFDM-IM}}(\gamma) < C_{\mathrm{OFDM}}(\gamma), \ \forall m > 0 \quad (43)$$

where

$$C_{\mathrm{OFDM}}(\gamma) = \frac{1}{L} \sum_{i=1}^{L} \log_2 \left(1+\gamma|h_i|^2\right) \quad (44)$$

denotes the instantaneous capacity of classical OFDM [29], [30].

Proof: Under Gaussian input, the PDF of the received signal on the i-th subcarrier conditioned on the channel is given by

$$f(y_i|h_i) = \frac{1}{\pi\sigma^2} \left[\frac{(L-m)^2}{L} \frac{1}{L-m+\gamma|h_i|^2 L} \times e^{-\frac{(L-m)|y_i|^2}{\sigma^2\left(L-m+\gamma|h_i|^2 L\right)}} + \frac{m}{L} e^{-\frac{|y_i|^2}{\sigma^2}} \right] \quad (45)$$

where $i = 1, \ldots, L$. In light of (45), it can be readily proved that the mean of y_i conditioned on h_i is zero and its variance yields

$$\begin{aligned} E_{y_i|h_i}\left[|y_i|^2\right] &= \frac{L-m}{L}\sigma^2 \left(1 + \frac{\gamma|h_i|^2 L}{L-m}\right) + \frac{m}{L}\sigma^2 \\ &= \frac{|h_i|^2 P_G}{L} + \sigma^2. \end{aligned} \quad (46)$$

Since the differential entropy of a zero-mean non-Gaussian RV is always smaller than that of a zero-mean Gaussian RV of the same variance [31], it follows that

$$\mathrm{h}(y_i|h_i) \le \log_2 \left(\pi e \sigma^2 \left(\gamma|h_i|^2 + 1 \right) \right) \quad (47)$$

with equality iff $m = 0$ which corresponds to the classical OFDM case. Then, according to [31, Theorem 9.6.2], i.e.,

$$\mathrm{h}(\mathbf{y}|\mathbf{h}) \le \mathrm{h}(y_1|h_1) + \cdots + \mathrm{h}(y_L|h_L) \quad (48)$$

with equality iff the received signals at all subcarriers conditioned on the channel are independent, and $\mathrm{I}(\mathbf{x}_s, \mathbf{x}_c; \mathbf{y}|\mathbf{h}) = \mathrm{h}(\mathbf{y}|\mathbf{h}) - L\log_2(\pi e\sigma^2)$, we arrive at (43), completing the proof. ■

Remark 4: In OFDM-IM, the power of the received signal on each subcarrier remains the same as that of classical OFDM. The distribution of the received signal, however, is not Gaussian. This differs from classical OFDM, thus leading to a smaller instantaneous capacity.

Having the conditional capacity of OFDM-IM in (38), we can then calculate the ergodic capacity of OFDM-IM, denoted by $\overline{C}_{\mathrm{OFDM-IM}}(\gamma)$, by averaging the channel realizations. Numerical results will be presented in Section V. From Proposition 3, it is expected that the ergodic capacity of OFDM-IM will always be smaller than that of classical OFDM. This can be explained alternatively by the fact that the parallel channels resulting from OFDM-IM are rank-reduced, while the ergodic capacity of a vector Gaussian channel is achieved if and only if the channel has full rank.

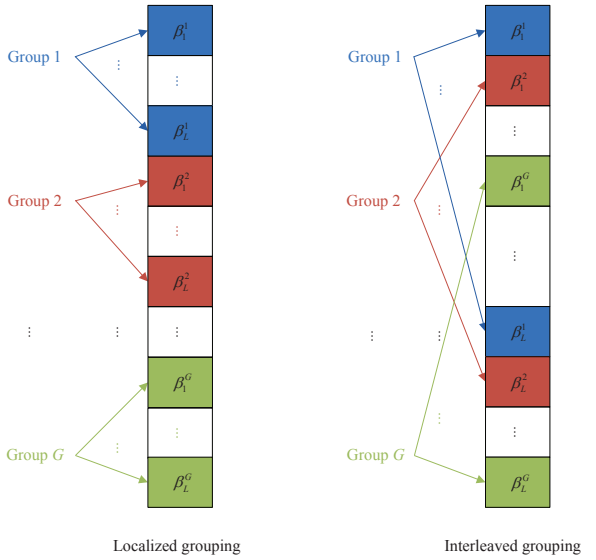

Fig. 2. Localized grouping vs. interleaved grouping.

IV. Interleaved Grouping

In this section, we answer $Q1$ raised in Section II.

Motivated by the derived lower bound on the achievable rate of OFDM-IM in Section III, which reveals that the correlation among channel coefficients on the subcarriers within a subcarrier group plays a key role, we propose a new subcarrier grouping approach for OFDM-IM to improve the performance of OFDM-IM. Unlike the previous OFDM-IM scheme, in which the subcarrier grouping is performed in a localized manner [18]–[20], we suggest grouping the subcarriers in an interleaved manner, as shown in Fig. 2. After interleaved grouping, the set of subcarrier indices for subcarrier group g will be given by

$$\Psi^g = \{\beta_1^g, \ldots, \beta_L^g\} = \{g, \ldots, g + (L-1)\,G\} \tag{49}$$

with $\beta_l^g = g + (l-1)\,G$, where $g = 1, \ldots, G$ and $l = 1, \ldots, L$. Note that when interleaved grouping is employed at the transmitter, it should be followed at the receiver. It is evident that applying either subcarrier grouping rule, i.e., localized grouping or interleaved grouping, leads to the same overall system complexity. Also note that from (49), it is clear that interleaved grouping is a kind of regular subcarrier grouping approaches since the (a,b)-th entry of the covariance matrix of $\mathbf{h}^g$ is $[\mathbf{\Sigma}_{\mathrm{IG}}]_{a,b} = \sum_{d=1}^{D} \delta_d^2 e^{-2\sqrt{-1}\pi(a-b)(d-1)/L}$ with $a, b = 1, \ldots, L$, which does not depend on g. Therefore, the analysis conducted in Section III also applies to interleaved grouping. The reason for adopting interleaved grouping is clarified in the following proposition.

Proposition 4: OFDM-IM with interleaved grouping achieves the highest information rate in both low and high SNR regions when the spacing of any two subcarriers within a subcarrier group is no smaller than the coherence bandwidth of the channel.

Proof: When SNR is either low or high, it follows from [23] that

$$\begin{aligned} R_{\mathrm{OFDM-IM}}(\gamma) \approx & \frac{L-m}{L}\log_2(M) + \frac{\log_2(\mathrm{C}(L,m))}{L} \\ & - \frac{1}{L\mathrm{C}(L,m)}\frac{1}{M^{L-m}} \sum_{j=1}^{\mathrm{C}(L,m)} \sum_{p^{(L-m)}} \\ & \times \log_2\left(\sum_{j'=1}^{\mathrm{C}(L,m)} \sum_{p'^{(L-m)}} \frac{1}{\det(\mathbf{I}_L + \mathbf{\Sigma}\mathbf{\Lambda}_{j,j'})}\right) \end{aligned} \tag{50}$$

where $\mathbf{\Lambda}_{j,j'}$ is defined in (26). Note that it is straightforward to have (50) according to Corollary 1 and Corollary 3. From (50), the optimal $\mathbf{\Sigma}^*$, which maximizes the achievable rate of OFDM-IM, lies in the following:

$$\begin{aligned} \mathbf{\Sigma}^* = & \arg\min_{\forall \mathbf{\Sigma}} \sum_{j=1}^{\mathrm{C}(L,m)} \sum_{p^{(L-m)}} \\ & \times \log_2\left(\sum_{j'=1}^{\mathrm{C}(L,m)} \sum_{p'^{(L-m)}} \frac{1}{\det(\mathbf{I}_L + \mathbf{\Sigma}\mathbf{\Lambda}_{j,j'})}\right). \end{aligned} \tag{51}$$

To solve (51), let us assume that the diagonal elements of $\mathbf{\Lambda}_{j,j'}$ are all positive. In this case, from [31, Theorem 16.8.2] (i.e., Hadamard's inequality), we have

$$\begin{aligned} \frac{1}{\det(\mathbf{I}_L + \mathbf{\Sigma}\mathbf{\Lambda}_{j,j'})} &= \frac{1}{\det\left(\mathbf{\Lambda}_{j,j'}^{-1} + \mathbf{\Sigma}\right)\det(\mathbf{\Lambda}_{j,j'})} \\ &\geq \prod_{i=1}^{L} \frac{1}{1 + [\mathbf{\Lambda}_{j,j'}]_{i,i}} \end{aligned} \tag{52}$$

with equality iff $\mathbf{\Sigma} = \mathbf{I}_L$, which represents the case in which $\mathbf{h}^g$ is a fully independent random vector. Since the logarithmic function is monotonically increasing, we obtain $\mathbf{\Sigma}^* = \mathbf{I}_L$.

However, the above assumption does not hold since, as shown in (27), there is at least one zero among the diagonal elements of $\mathbf{\Lambda}_{j,j'}$. Despite this, we will see that the solution, i.e., $\mathbf{\Sigma}^* = \mathbf{I}_L$, is still valid. To show this, first assume that only one diagonal element of $\mathbf{\Lambda}_{j,j'}$, e.g., $[\mathbf{\Lambda}_{j,j'}]_{k,k}$, equals zero. In this case, we can eliminate the k-th row as well as the k-th column of $\mathbf{\Sigma}$ and $\mathbf{\Lambda}_{j,j'}$, yielding updated $\widetilde{\mathbf{\Sigma}}$ and $\widetilde{\mathbf{\Lambda}}_{j,j'}$. Consequently, it follows from [31, Theorem 16.8.2] that

$$\begin{aligned} \frac{1}{\det(\mathbf{I}_L + \mathbf{\Sigma}\mathbf{\Lambda}_{j,j'})} &= \frac{1}{\det\left(\widetilde{\mathbf{\Lambda}}_{j,j'}^{-1} + \widetilde{\mathbf{\Sigma}}\right)\det\left(\widetilde{\mathbf{\Lambda}}_{j,j'}\right)} \\ &\geq \prod_{i=1, i\neq k}^{L} \frac{1}{1 + [\mathbf{\Lambda}_{j,j'}]_{i,i}} \\ &= \prod_{i=1}^{L} \frac{1}{1 + [\mathbf{\Lambda}_{j,j'}]_{i,i}} \end{aligned} \tag{53}$$

with equality iff $\widetilde{\mathbf{\Sigma}} = \mathbf{I}_{L-1}$. Since for different $j, j' \in \{1, \ldots, \mathrm{C}(L,m)\}$, the location of the zero in the diagonal elements of $\mathbf{\Lambda}_{j,j'}$ spans from 1 to L, we achieve that $\mathbf{\Sigma}^* = \mathbf{I}_L$. In analogy with the above analysis, the same conclusion can be drawn when more diagonal elements of $\mathbf{\Lambda}_{j,j'}$ equal zero.

In order to achieve the maximum rate of OFDM-IM, the subcarriers within a subcarrier group should be spaced apart

in frequency as far as possible to benefit from the independent fading. It is easy to see that interleaved grouping meets this requirement most perfectly, thus completing the proof. ■

Remark 5: For double check, let us consider the special case in which the elements of $\mathbf{h}^g$ are highly correlated, which usually happens to the localized grouping method when the bandwidth spanned by the L continuous subcarriers is smaller than the coherence bandwidth of the channel. From Corollary 2 and the identity $(1+\mathrm{Tr}\{\mathbf{\Lambda}_{j,j'}\})^{-1} > \prod_{i=1}^{L}(1+[\mathbf{\Lambda}_{j,j'}]_{i,i})^{-1}$, it is easy to verify that the resulting achievable rate is smaller than that of the independent case.

Remark 6: In practical systems, the condition in Proposition 4 can be satisfied. Take LTE systems for example. In a macrocell, the coherence bandwidth is on the order of 1 MHz [13]. Therefore, for a system bandwidth of 20 MHz, the subcarriers within each subcarrier group after interleaved grouping will experience independent fading provided that $L < 20$. Since as will be disclosed in Section V, the superiority of OFDM-IM over classical OFDM narrows as the alphabet size of the signal input grows, $L < 20$ is advantageous for OFDM-IM.

Remark 7: Since $\overline{C}_{\mathrm{OFDM-IM}}(\gamma)$ is dominated by the expectation of $\mathrm{I}(\mathbf{x}_s;\mathbf{y}|\mathbf{x}_c,\mathbf{h})$ over $\mathbf{h}$ with $\mathbf{x}_s$ being a Gaussian signal set (especially as SNR gets higher), which is independent of the channel correlation as (39) implies, the gap between the resulting ergodic capacity of localized grouping and interleaved grouping will be very small. Furthermore, considering that Gaussian input is unfavorable to OFDM-IM with respect to classical OFDM as analyzed earlier, we do not evaluate the aforementioned gap in this paper.

Remark 8: From (26) and the proof for Proposition 4, we see that the lower bound on the achievable rate of OFDM-IM achieves its maximum when $\mathbf{\Sigma} = \mathbf{I}_L$, i.e., subcarriers within a subcarrier group are faded independently. Therefore, we expect that the interleaved grouping will also perform better than the localized grouping in the moderate SNR region for PSK/QAM-constrained input. This will be validated in the following section.

V. Numerical Results and Discussions

In this section, numerical results are presented to validate the analysis and make comparisons between classical OFDM and OFDM-IM. The achievable rate is chosen as the performance metric.

A. Localized grouping vs. interleaved grouping

In this subsection, we answer *Q1*, *Q2* raised in Section II.

In the numerical calculations, the total number of subcarriers is chosen as $N = 64$ and the channel is assumed to have an exponentially decaying power delay profile with $\delta_d^2 = e^{-(d-1)}/\sum_{u=1}^{D} e^{-(u-1)}$ and $D = 10$ taps, where $d = 1,\ldots,D$. The results are shown in Figs. 3 and 4, where the parameters are chosen as: $L = 2$, $m = 1$, and BPSK in Fig. 3(a); $L = 4$, $m = 1$, and QPSK in Fig. 3(b); $L = 8$, $m = 1$, and 8-PSK in Fig. 4(a); $L = 16$, $m = 1$, and 16-PSK in Fig. 4(b). To see how OFDM-IM compares with classical OFDM, the performance of classical OFDM employing the same alphabet for symbol modulation as OFDM-IM is also depicted. It is noted that the OFDM-IM with $L = 2$, $m = 1$, and localized grouping is exactly the ESIM-OFDM scheme [18]. Also note that the OFDM-IM and the classical OFDM in Figs. 3 and 4 share the same entropy at the channel input. As seen from the figures, unlike classical OFDM for which the grouping type is irrelevant to performance, OFDM-IM with interleaved grouping can achieve up to 3 dB, 2 dB, 0.5 dB, and 0.2 dB SNR gains over OFDM-IM with localized grouping at achievable rates equal to 0.95 bps/Hz in Fig. 3(a), 1.85 bps/Hz in Fig. 3(b), 2.6 bps/Hz in Fig. 4(a), and 2.8 bps/Hz in Fig. 4(b), respectively. This is expected because the independence of channel fading makes the different subcarrier

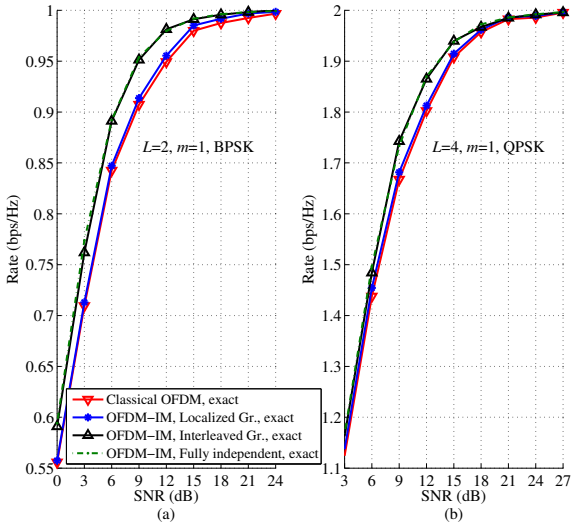

Fig. 3. Comparison between classical OFDM and OFDM-IM with localized grouping and interleaved grouping in terms of achievable rate with parameters chosen as: (a) $L = 2$, $m = 1$, BPSK; (b) $L = 4$, $m = 1$, QPSK.

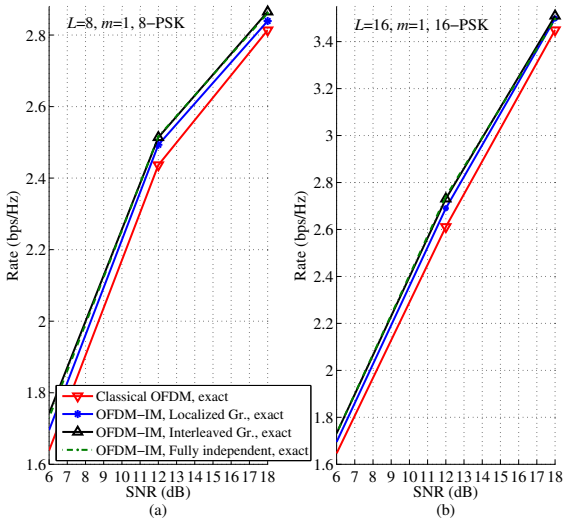

Fig. 4. Comparison between classical OFDM and OFDM-IM with localized grouping and interleaved grouping in terms of achievable rate with parameters chosen as: (a) $L = 8$, $m = 1$, 8-PSK; (b) $L = 16$, $m = 1$, 16-PSK.

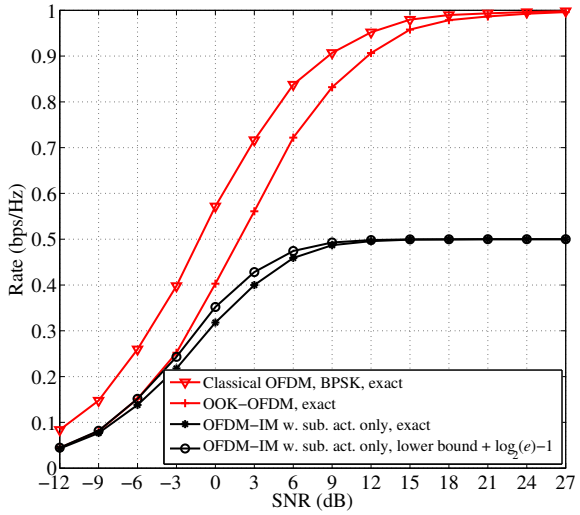

Fig. 5. Performance comparison between classical OFDM with BPSK, OOK-OFDM, and OFDM-IM with subcarrier activation only.

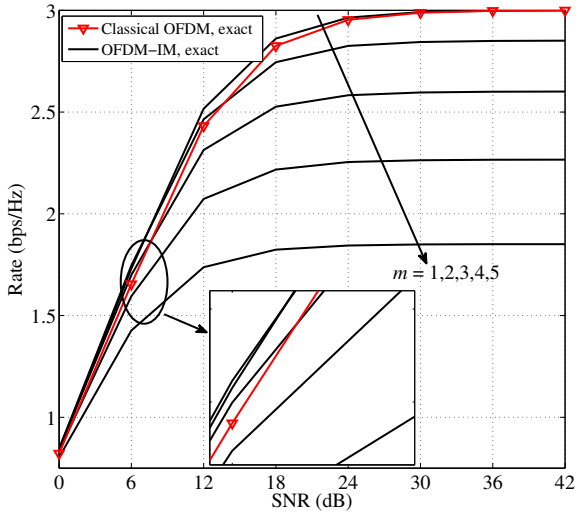

Fig. 6. Comparison between classical OFDM and OFDM-IM with $L = 8$ and 8-PSK.

activation types easier to differentiate, which in turn improves the coding gain from index modulation. On the other hand, at those achievable rates, OFDM-IM with interleaved grouping outperforms classical OFDM with an SNR gain of up to 3 dB. From the figures, we also see that the resulting achievable rates by interleaved grouping from the practical channel model match the ultimate ones derived by assuming fully independent fading, perfectly. This is in consistent with Proposition 3 as in those cases the interleaved grouping ensures the channel coefficients on subcarriers within a subcarrier group are approximately statistically independent.

Since as validated above the ultimate performance of OFDM-IM is available by adopting interleaved grouping in practice, in the following subsections we will simply let the subcarriers within each subcarrier group experience independent fading in order to examine the ultimate performance of OFDM-IM and avoid channel particularity.

B. Performance of OFDM-IM with subcarrier activation only

In this subsection, we answer *Q3* raised in Section II.

With the aid of (35) and (36), we compute the achievable rates of OFDM-IM with subcarrier activation only, classical OFDM with BPSK, and OOK-OFDM, in Fig. 5. To examine the constant-shifted method mentioned in Section III.A, we add $\log_2(e) - 1$ to the lower bound on the achievable rate of OFDM-IM with subcarrier activation only. As seen from the figure, this constant-shifted lower bound overestimates the exact value in the moderate SNR region, though it achieves a perfect approximation at both low and high SNRs. Therefore, this method is infeasible in practice. Regarding the performance of these three schemes, we can conclude from Fig. 5 that classical OFDM with BPSK outperforms the other two schemes while OFDM-IM with subcarrier activation only performs worse in general though it exhibits similar performance to OOK-OFDM in the very low SNR region. The positive result associated with classical OFDM with BPSK can be accounted for its 3 dB larger minimum Euclidean distance than OOK-OFDM and its double entropy at the channel input over OFDM-IM with subcarrier activation only. The behavior of OFDM-IM with subcarrier activation only in the very low SNR region can be attributed to the coding gain from index modulation.

C. Performance of different subcarrier activation strategies

In this subsection, we answer *Q4* raised in Section II.

In Figs. 3 and 4, we observe interestingly that OFDM-IM with $m = 1$ surpasses classical OFDM significantly under the finite constellation constraints. However, since the decoding reliability of the modulated symbol varies with the constellation order under a power constraint and that of different subcarrier activation types varies with the parameters L and m, different phenomena will be observed for different system parameters.

To show this, we present an example with $L = 8$ and 8-PSK in Fig. 6, where m varies from 1 to 5. As can be seen, besides $m = 1$, in which case OFDM-IM and classical OFDM have the same entropy at the channel input, OFDM-IM with $m = 2$ and $m = 3$ also have the potential to outperform classical OFDM despite smaller input entropy. For $m = 4$ and 5, the input entropies are too small to exploit the channel, thus leading to a smaller achievable rate than classical OFDM. Therefore, an intriguing question may arise: what is the optimal m in maximizing the achievable rate for a given SNR. For the above example, answers are given in Fig. 7, where SNRs equal to 0 dB, 6 dB, and 12 dB are considered, and the corresponding lower bounds are also plotted. It is shown that there exists an optimal non-zero m (marked with a circle) which may vary for different SNR values. However, we expect in general that when SNR becomes very high the optimal m is more likely to be 1 since the entropy at the channel input is the largest. On the other

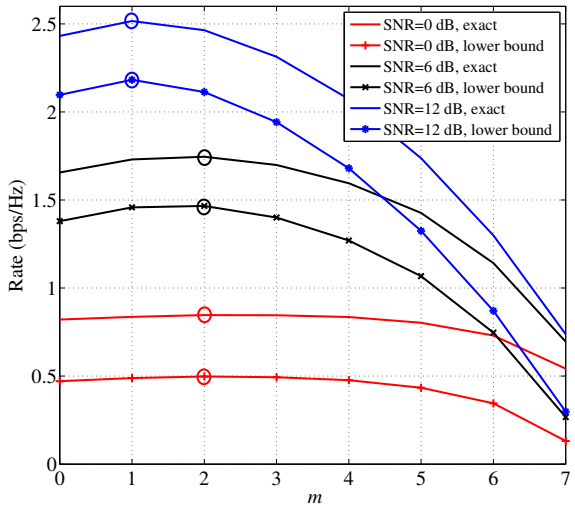

Fig. 7. Effect of m on the achievable rate in the case of $L = 8$, 8-PSK, and SNRs equal to 0 dB, 6 dB, and 12 dB, respectively.

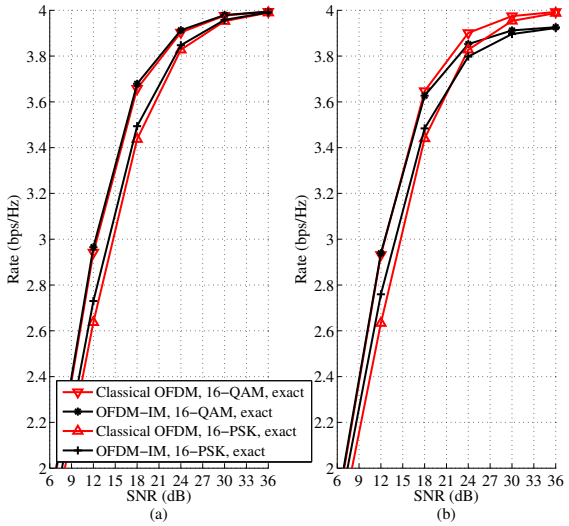

Fig. 8. Effect of modulation types on the achievable rates of classical OFDM and OFDM-IM with $L = 16$ and (a) $m = 1$; (b) $m = 2$.

hand, it is clear from Fig. 7 that the proposed lower bound can also point out the same solutions for its potential to trace the exact values as the increase of SNR well (see Fig. 5 for more evidences). Therefore, for computational tractability, the use of the proposed lower bound is more advisable in the determination of the optimal m. It is worth noting that under a finite-alphabet input, the achievable rates of all schemes will always saturate at their corresponding uncoded transmitted information rates at very high SNR.

D. PSK vs. QAM

In this subsection, we answer *Q5* raised in Section II.

An example for the comparison between 16-PSK and 16-QAM inputs is shown in Fig. 8, where the simulation parameters are $L = 16$ and (a) $m = 1$; (b) $m = 2$. For

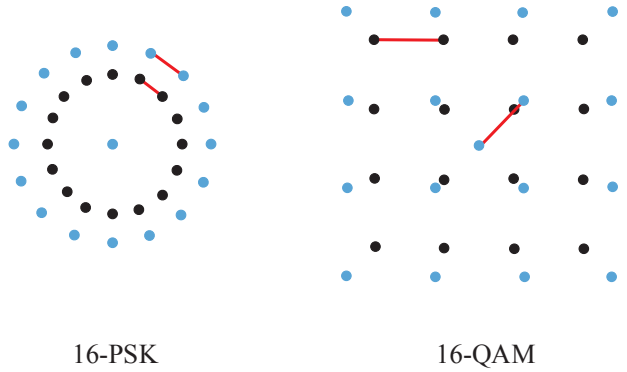

Fig. 9. Differences in the minimum Euclidean distances associated with classical OFDM and OFDM-IM for 16-PSK and 16-QAM constrained inputs, where the black and blue points, respectively, belong to the constellations of classical OFDM and OFDM-IM, and the red lines give the minimum Euclidean distances.

figure clarity, the lower bounds are omitted. Different from the conclusion drawn in spatial modulation that PSK may be better than QAM [35], [36], from the figure we see that QAM is always more favorable than PSK for OFDM-IM in the sense of higher achievable rate. On the other hand, we see that OFDM-IM with $m = 1$ and $m = 2$ shows an SNR gain of nearly 1 dB over classical OFDM for a large SNR range when both employ 16-PSK modulation whereas very little gain is found when both employ 16-QAM modulation. Reasons can be found by comparing the minimum Euclidean distances of the overall constellations of classical OFDM and OFDM-IM with 16-PSK and 16-QAM in Fig. 9. As seen from the figure, the overall constellations of OFDM-IM are different from those of classical OFDM. Particularly, in OFDM-IM, one more constellation point is located at the origin, which is introduced from the inactive state, and meanwhile a power gain of $L/(L-m)$ is shared by all conventional 16-PSK and 16-QAM constellation points. Therefore, the minimum Euclidean distance of the overall constellation of OFDM-IM with 16-PSK will still be determined by the two adjacent 16-PSK constellation points of enhanced power while that with 16-QAM will be determined by the origin point and its nearest 16-QAM constellation point of enhanced power. It should be noted that since in OFDM-IM the origin point appears with probability m/L while each 16-PSK/QAM constellation point appears with probability $(L-m)/ML$, the comparison through measuring the Euclidean distance directly need not guarantee absolute accuracy. However, this can be adopted as a general principle to foresee the comparison result when a larger alphabet, such as 64-PSK/QAM is considered.

E. Effects of Gaussian input

In this subsection, we compare the performance of OFDM-IM with classical OFDM under Gaussian input.

With $L = 8$ and m spanning from 1 to 7, the comparison in terms of ergodic capacity is illustrated in Fig. 10. The expectation of (39) over channels, which accounts for the portion of ergodic capacity contributed by symbol modulation,

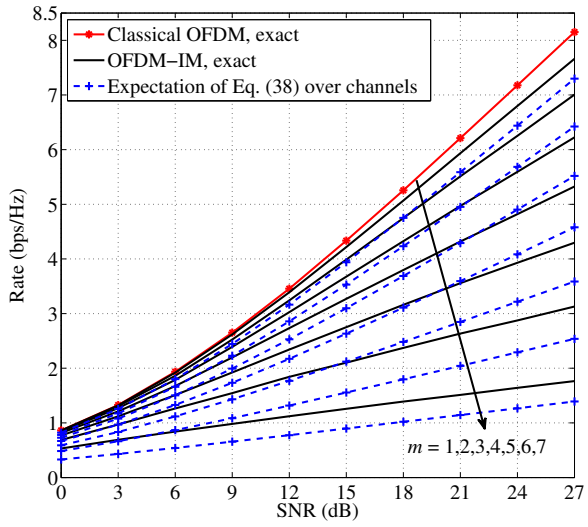

Fig. 10. Comparison between classical OFDM and OFDM-IM with $L = 8$ in terms of ergodic capacity.

is also depicted. As seen from the figure, the contribution of subcarrier activation to the ergodic capacity, which equals the gap between the black and blue dashed curves, cannot be neglected. Take $m = 4$ for example. At SNR equal to 27 dB, the ergodic capacity of OFDM-IM is about 5.3 bps/Hz and the portion contributed by symbol modulation is about 4.6 bps/Hz. Therefore, the other portion contributed by subcarrier activation is about $5.3 - 4.6 = 0.7$ bps/Hz, resulting in the ratio between the portions of the ergodic capacity contributed by subcarrier activation and symbol modulation as high as $0.7/4.6 = 15.2\%$. On the other hand, it is clear that the figure substantiates our conclusion presented in Section III.B that OFDM-IM performs worse than classical OFDM under Gaussian input.

VI. Conclusions

With the transmitted signal being drawn from a finite constellation, the achievable rate of OFDM-IM with CSIR has been studied and a lower bound in closed form has been derived. It has been verified that the derived lower bound can be used to predict the optimal subcarrier activation strategy which maximizes the superiority of OFDM-IM over classical OFDM. In addition, an interleaved grouping has been proposed and shown to outperform the existing localized grouping. Finally, the effects of modulation types on the performance of OFDM-IM have been studied.

References

[1] X. Cheng, B. Yu, L. Yang, J. Zhang, G. Liu, Y. Wu, and L. Wan, "Communicating in the real world: 3D MIMO," *IEEE Wireless Commun. Mag.*, vol. 21, no. 4, pp. 136–144, Aug. 2014.

[2] X. Cheng, C. -X. Wang, H. Wang, X. Gao, X. -H. You, D. Yuan, B. Ai, Q. Huo, L. Song, and B. Jiao, "Cooperative MIMO channel modeling and multi-link spatial correlation properties," *IEEE J. Sel. Areas in Commun.*, vol. 30, no. 2, pp. 388–396, Feb. 2012.

[3] R. Y. Mesleh, H. Haas, S. Sinanovic, C. W. Ahn, and S. Yun, "Spatial modulation," *IEEE Trans. Veh. Tech.*, vol. 57, no. 4, pp. 2228–2241, July 2008.

[4] Y. Abdelhamid, N. Serafimovski, R. Mesleh, and H. Haas, "Generalised spatial modulation," in *Proc. Asilomar Conf. Signals, Syst. Comput.*, Pacific Grove, CA, USA, Nov. 2010, pp. 1498-1502.

[5] M. Di Renzo, H. Haas, and P. M. Grant, "Spatial modulation for multiple-antenna wireless systems: A survey," *IEEE Commun. Mag.*, vol. 49, no. 12, pp. 182–191, Dec. 2011.

[6] Y. Bian, X. Cheng, M. Wen, L. Yang, H. V. Poor, and B. Jiao, "Differential spatial modulation," *IEEE Trans. Veh. Commun.*, vol. 64, no. 7, pp. 3262–3268, Jul. 2015.

[7] J. Jeganathan, A. Ghrayeb, L. Szczecinski, and A. Ceron, "Space shift keying modulation for MIMO channels," *IEEE Trans. Wireless Commun.*, vol. 8, no. 7, pp. 3692C3703, Jul. 2009.

[8] M. Wen, X. Cheng, H. V. Poor, and B. Jiao, "Use of SSK modulation in two-way amplify-and-forward relaying," *IEEE Trans. Veh. Tech.*, vol. 63, no. 3, pp. 1498-1504, Mar. 2014.

[9] M. Di Renzo, H. Haas, A. Ghrayeb, S. Sugiura, and L. Hanzo, "Spatial modulation for generalized MIMO: challenges, opportunities and implementation," *Proc. of the IEEE*, vol. 102, no. 1, pp. 56-103, Jan. 2014.

[10] A. Younis, W. Thompson, M. Di Renzo, C. -X. Wang, M. A. Beach, H. Haas, and P. M. Grant, "Performance of spatial modulation using measured real-world channels," in *Proc. IEEE Vehicular Technology Conference (VTC Fall)*, Las Vegas, NV, USA, Mar. 2013, pp. 1–5.

[11] N. Serafimovski, A. Younis, R. Mesleh, P. Chambers, M. Di Renzo, C. -X. Wang, P. M. Grant, M. A. Beach, and H. Haas, "Practical implementation of spatial modulation," *IEEE Trans. Veh. Tech.*, vol. 62, no. 9, pp. 4511–4523, Nov. 2013.

[12] J. Zhang, Y. Wang, L. Ding, and N. Zhang, "Bit error probability of spatial modulation over measured indoor channels," *IEEE Trans. Wireless Commun.*, vol. 13, no. 3, pp. 1380–1387, Mar. 2014.

[13] Telesystem Innovations, "LTE in a nutshell: System overview". White Paper, 2010.

[14] R. Mesleh, H. Haas, C. W. Ahn, and S. Yun, "Spatial modulation-OFDM," in *Proc. 11th International OFDM-Workshop 2006 (InOWo'06)*, Hamburg, Germany, Aug. 2006, pp. 288–292.

[15] S. Ganesan, R. Mesleh, H. Haas, C. W. Ahn, and S. Yun, "On the performance of spatial modulation OFDM," in *Proc. Asilomar Conf. Signals, Syst. Comput.*, Pacific Grove, CA, USA, Nov. 2006, pp. 1825–1829.

[16] R. Mesleh, S. Gansean, and H. Haas, "Impact of channel imperfections on spatial modulation OFDM," in *Proc. IEEE 18th International Symposium on Personal, Indoor and Mobile Radio Communications (PIMRC)*, Athens, Greece, Mar. 2007, pp. 1-5.

[17] R. A.Alhiga and H. Haas, "Subcarrier-index modulation OFDM," in *Proc. IEEE 20th International Symposium on Personal, Indoor and Mobile Radio Communications (PIMRC)*, Tokyo, Japan, Sept. 2009, pp. 177-181.

[18] D. Tsonev, S. Sinanovic, and H. Haas, "Enhanced subcarrier index modulation (SIM) OFDM," in *Proc. IEEE Global Communications Conference (GLOBECOM) Workshops*, Houston, TX, USA, Dec. 2011, pp. 728-732.

[19] E. Basar, U. Aygolu, E. Panayirci, and H. V. Poor, "Orthogonal frequency division multiplexing with index modulation," in *Proc. IEEE Global Communications Conference (GLOBECOM)*, Anahem, CA, USA, Dec. 2012, pp. 4741-4746.

[20] E. Basar, U. Aygolu, E. Panayirci, and H. V. Poor, "Orthogonal frequency division multiplexing with index modulation," *IEEE Trans. Signal Process.*, vol. 61, no. 22, pp. 5536-5549, Nov. 2013.

[21] G. Ungerboeck, "Channel coding with multilevel/phase signals," *IEEE Trans. Inf. Theory*, vol. 28, no. 1, pp. 55-67, 1982.

[22] W. He and C. N. Georghiades, "Computing the capacity of a MIMO fading channel under PSK signaling," *IEEE Trans. Inf. Theory*, vol. 51, no. 5, pp. 1794–1803, May 2005.

[23] J. Harshan and B. S. Rajan, "On two-user Gaussian multiple access channels with finite input constellations," *IEEE Trans. Inf. Theory*, vol. 57, no. 3, pp. 1299–1327, Mar. 2011.

[24] W. Zeng, C. Xiao, and J. Lu, "A low-complexity design of linear precoding for MIMO channels with finite-alphabet inputs," *IEEE Wireless Commun. Lett.*, vol. 1, no. 1, pp. 38–41, Feb. 2012.

[25] C. Xiao, Y. R. Zheng, and Z. Ding, "Globally optimal linear precoders for finite alphabet signals over complex vector Gaussian channels," *IEEE Trans. Signal Process.*, vol. 59, no. 7, pp. 3301–3314, July 2011.

[26] M. Wen, X. Cheng, M. Wang, B. Ai, and B. Jiao, "Error probability analysis of interleaved SC-FDMA systems over Nakagami-m frequency selective fading channels," *IEEE Trans. Veh. Tech.*, vol. 62, no. 2, pp. 748–761, Feb. 2013.

[27] J. R. Hershey and P. A. Olsen, "Approximating the Kullback-Leibler divergence between Gaussian mixture models," in *Proc. IEEE International Conference on Acoustics, Speech and Signal Processing (ICASSP)*, Honolulu, HI, USA, Apr. 2007, pp. IV-317–IV-320.
[28] L. Zhao, H. Zhao, K. Zheng, and Y. Yang, "A high energy efficient scheme with selecting sub-carriers modulation in OFDM system," in *Proc. IEEE International Conference on Communications (ICC)*, Ottawa, ON, 2012, pp. 5711–5715.
[29] D. Tse and P. Viswanath, *Fundamentals of Wireless Communications*, Cambridge University Press, 2005.
[30] H. Bolcskei, D. Gesbert, and A. J. Paulraj, "On the capacity of OFDM-based spatial multiplexing systems," *IEEE Trans. Commun.*, vol. 50, no. 2, pp. 225-234, Feb. 2002.
[31] T. M. Cover and J. A. Thomas, *Elements of Information Theory*, 2nd ed. New York: Wiley, 2006.
[32] I. S. Gradshteyn and I. M. Rhyhik, *Table of Integrals, Series and Products*, 7th ed. New York: Academic, 2007.
[33] J. M. Kahn and J. R. Barry, "Wireless infrared communications," *Proc. of the IEEE*, vol. 85, no. 2, pp. 265-298, Feb. 1997.
[34] Y. Yang and B. Jiao, "Information-guided channel-hopping for high data rate wireless communication," *IEEE Commun. Lett.*, vol. 12, no. 4, pp. 225–227, Apr. 2008.
[35] M. Di Renzo and H. Haas, "Bit error probability of SM-MIMO over generalized fading channels," *IEEE Trans. Veh. Tech.*, vol. 61, no. 3, pp. 1124–1144, Mar. 2012.
[36] P. Yang, M. Di Renzo, Y. Xiao, S. Li, and L. Hanzo, "Design guidelines for spatial modulation," *IEEE Commun. Surveys & Tutorials*, vol. 17, no. 1, pp. 6–26, First Quarter 2015.
[37] W. Zeng, C. Xiao, M. Wang, and J. Lu, "Linear precoding for finite-alphabet inputs over MIMO fading channels with statistical CSI," *IEEE Trans. Signal Process.*, vol. 60, no. 6, pp. 3134–3148, June 2012.

Miaowen Wen (M'14) received the B.S. degree from Beijing Jiaotong University, Beijing, China, in 2009, and Ph.D. degree from Peking University, Beijing, China, in 2014. From September 2012 to September 2013, he was a Visiting Student Research Collaborator with Princeton University, Princeton, NJ, USA. Since September 2014, he has been on the faculty of South China University of Technology, Guangzhou, China.

Dr. Wen has published more than 40 papers in refereed journals and conference proceedings. His recent research interests include spatial modulation and non-orthogonal multiple access techniques. He was a recipient of the Best Paper Award from the IEEE International Conference on Intelligent Transportation Systems Telecommunications 2012 and the IEEE International Conference on Intelligent Transportation Systems 2014.

Xiang Cheng (S'05-M'10-SM'13) received the Ph.D. degree from Heriot-Watt University, Edinburgh, U.K., and The University of Edinburgh, Edinburgh, in 2009.

Since 2010, he has been with Peking University, Beijing, China, first as a Lecturer and then as an Associate Professor. He is the author of more than 120 research papers in journals and conference proceedings. His research interests include mobile propagation channel modeling and simulation, next generation mobile cellular systems, intelligent transport systems, and hardware prototype development.

Dr. Cheng was a Symposium Leading Chair, a Cochair, and a member of the technical program committees of several international conferences. He is currently an Associate Editor of the IEEE TRANSACTIONS ON INTELLIGENT TRANSPORTATION SYSTEMS. He was a recipient of the Postgraduate Research Thesis Prize for his Ph.D. study, the 2009 Chinese National Award for Outstanding Overseas Ph.D. Students for his academic excellence and outstanding performance, and the Best Paper Award from the IEEE International Conference on Intelligent Transportation Systems Telecommunications 2012, the IEEE International Conference on Communications in China 2013, and the IEEE International Conference on Intelligent Transportation Systems 2014.

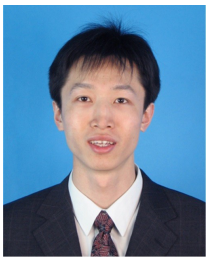

Meng Ma was born in Harbin, China, in 1978. He received B.S. and Ph.D. degrees in Electrical Engineering from Peking University, in 2001 and 2007, respectively. He is an Associate Professor with the School of Electronics Engineering and Computer Science, Peking University, Beijing, China. From January 2009 to January 2010, he was a visiting scholar at Commonwealth Scientific and Industrial Research Organization (CSIRO), Sydney, Australia. His research interests include transmitter and receiver signal processing. He has published over 40 papers in refereed journals and conference proceedings. He holds twenty patents in wireless technologies.

Bingli Jiao received B.S. and M.S. degree from Peking University, China in 1983 and 1988, respectively, and received Ph.D. from University of Sarrbruecken, F. R., Germany in 1995. Then, he became an associate professor and professor with Peking University in 1995 and 2000, respectively. His current interests include communication theory and techniques and sensor design.

H. Vincent Poor (S'72, M'77, SM'82, F'87) received the Ph.D. degree in EECS from Princeton University in 1977. From 1977 until 1990, he was on the faculty of the University of Illinois at Urbana-Champaign. Since 1990 he has been on the faculty at Princeton, where he is the Michael Henry Strater University Professor of Electrical Engineering and Dean of the School of Engineering and Applied Science. Dr. Poors research interests are in the areas of statistical signal processing, stochastic analysis and information theory, and their applications in wireless networks and related fields. Among his publications in these areas is the recent book Mechanisms and Games for Dynamic Spectrum Allocation (Cambridge University Press, 2014).

Dr. Poor is a member of the National Academy of Engineering and the National Academy of Sciences, and a foreign member of Academia Europaea and the Royal Society. He is also a fellow of the American Academy of Arts and Sciences, the Royal Academy of Engineering (U. K), and the Royal Society of Edinburgh. He received the Technical Achievement and Society Awards of the IEEE Signal Processing Society in 2007 and 2011, respectively. Recent recognition of his work includes the 2014 URSI Booker Gold Medal, the 2015 EURASIP Athanasios Papoulis Award, and honorary doctorates from Aalborg University, Aalto University, HKUST and the University of Edinburgh.